photonics

MDPI

Article

Prompt Analysis and Design for Passively Mode-Locked Solid-State Lasers with Semiconductor Saturable Absorbers

Pin-Wen Cheng [1], Yu-Hsin Hsu [1], Hsing-Chih Liang [2], Kai-Feng Huang [1] and Yung-Fu Chen [1,*]

[1] Department of Electrophysics, National Yang Ming Chiao Tung University, Hsinchu 30010, Taiwan; windrc.sc10@nycu.edu.tw (P.-W.C.); yuhsin.sc10@nycu.edu.tw (Y.-H.H.); kfhuang@nycu.edu.tw (K.-F.H.)
[2] Institute of Physics, National Yang Ming Chiao Tung University, Hsinchu 30010, Taiwan; hcliang@nycu.edu.tw
* Correspondence: yfchen@nycu.edu.tw

Abstract: The critical pump power for achieving passively continuous-wave mode-locking in a solid-state laser is analytically derived from the spatially dependent rate equations and the criterion for the intracavity pulse energy. A prompt way is proposed to straightforwardly design the cavity for passively mode-locked solid-state lasers. Complete experiments are performed to demonstrate the proposed cavity design and, simultaneously, to verify the theoretical model for the critical pump powers. It is interestingly observed that even though a larger modulation depth causes a higher critical pump power, it can generate a shorter pulse width in return.

Keywords: diode-pumped; passive mode-locking; solid-state laser; critical pump power

check for updates

Citation: Cheng, P.-W.; Hsu, Y.-H.; Liang, H.-C.; Huang, K.-F.; Chen, Y.-F. Prompt Analysis and Design for Passively Mode-Locked Solid-State Lasers with Semiconductor Saturable Absorbers. *Photonics* **2024**, *11*, 8. https://doi.org/10.3390/photonics11010008

Received: 1 December 2023
Revised: 18 December 2023
Accepted: 21 December 2023
Published: 22 December 2023

Copyright: © 2023 by the authors. Licensee MDPI, Basel, Switzerland. This article is an open access article distributed under the terms and conditions of the Creative Commons Attribution (CC BY) license (https://creativecommons.org/licenses/by/4.0/).

1. Introduction

Continuous-wave mode-locked (CWML) solid-state lasers have opened up a variety of applications including high-precision machining [1], nonlinear frequency conversion [2–4], and advanced laser spectroscopy [5,6]. The approaches used to achieve mode-locked lasers can be categorized into "active" and "passive" technologies. Actively mode-locking usually involves the use of an acousto-optical or electro-optical device to modulate the laser inside the cavity, leading to more components and compromising the flexibility and robustness of the cavity. In contrast, passively mode-locking does not utilize the active device but uses the nonlinearity of the saturable absorber to modulate the cavity light through real optical materials with nonlinear absorption properties, making the design more flexible and robust [7–10]. Saturable absorbers, such as a semiconductor saturable absorber mirror (SESAM) can be exploited to generate passive Q-switching or mode-locking, which should be distinguished from the Q-switched mode-locking (QML), known as the Q-switching instability, which often leads to unstable lasing operation in solid-state mode-locked lasers [11–13]. In the QML operation, the laser output obviously displays the feature of the mode-locked pulse train in a Q-switched envelope. Hönninger et al. [11] used the rate equations with a linearized stability analysis to obtain a stability criterion against QML. The criterion reveals that there is a critical intracavity pulse energy, $E_{P,C}$, for achieving a stable CWML operation. When the intracavity energy E_P of the mode-locked pulse is smaller than the critical energy $E_{P,C}$, the laser is stated in the QML. On the contrary, the CWML operation can be achieved for $E_P > E_{P,C}$. Hönninger et al. [11] derived the critical intracavity pulse energy $E_{P,C}$ as

$$E_{P,C} = \left(F_{sat,L} A_{eff,L} F_{sat,A} A_{eff,A} \Delta R\right)^{1/2}, \quad (1)$$

where $F_{sat,L}$ is the saturation fluence of the gain medium, $A_{eff,L}$ is the effective laser mode area inside the gain medium, $F_{sat,A}$ is the saturation fluence of the saturable absorber,

$A_{eff,A}$ is the effective laser mode area inside the saturable absorber, and ΔR is the modulation depth of the absorber. The saturation fluence of the gain medium is given by $F_{sat,L} = h\nu_l/m\sigma$, where $h\nu_l$ is the lasing photon energy, σ is the stimulated emission cross-section, and the factor m is the number of passes through the gain element per cavity round trip. For a ring cavity, $m = 1$, while for a simple standing wave cavity, $m = 2$. From the practical requirement, the critical pump power is more straightforward than the critical energy to evaluate the feasibility of achieving CWML. Furthermore, as seen from Equation (1), the mode areas $A_{eff,L}$ and $A_{eff,A}$ should be carefully designed to control the critical pump power. Therefore, it will be greatly desirable to develop a prompt way for designing $A_{eff,L}$ and $A_{eff,A}$ to fulfill CWML solid-state lasers. The study here is on a real saturable absorber rather than an artificial saturable absorber [14,15]. Examples of artificial saturable absorbers include nonlinear polarization rotation, the principle of the Mamyshev regenerator, and a nonlinear optical loop mirror. As usual, artificial saturable absorbers are vulnerable and susceptible to environmental conditions such as fiber movement, temperature, and vibration. In addition, artificial saturable absorbers usually exhibit random birefringence and polarization, which makes it difficult to design robust laser cavities.

In this work, we derive an analytical equation to express the output power as a function of the pump power based on the spatially dependent rate equations. We further combine the derived equation with the critical intracavity pulse energy to obtain an analytical expression for the critical pump power for achieving CWML. Moreover, we develop a prompt scheme to straightforwardly design the cavity for passively mode-locked solid-state lasers. We perform thorough experiments to demonstrate the developed scheme and, simultaneously, to verify the theoretical analysis for the critical pump powers. In the experiment, we intriguingly find that a larger modulation depth leads to a higher critical pump power, but it can bring about a shorter pulse width in return.

2. Theoretical Model

The spatially dependent rate equation for the population density is given by [16,17]

$$\frac{d\,n(\mathrm{r},t)}{dt} = \rho_p(\mathrm{r},t) - c\sigma\,\phi(\mathrm{r},t)\;n(\mathrm{r},t) - \frac{n(\mathrm{r},t)}{\tau_f}, \tag{2}$$

where $n(\mathrm{r},t)$ is the upper state population density, $\phi(\mathrm{r},t)$ is the spatial distribution of the cavity photons, $\rho_p(\mathrm{r},t)$ is the spatial distribution of the pump rate, s is the stimulated emission cross-section, and τ_f is the upper-level lifetime. In terms of the normalized pump distribution $\rho_o(\mathrm{r})$, the intensity $n(\mathrm{r},t)$ and distribution $\rho_p(\mathrm{r},t)$ can be expressed as $n(\mathrm{r},t) = N\rho_o(\mathrm{r})$ and $\rho_p(\mathrm{r},t) = R_p\,\rho_o(\mathrm{r})$, where N is the total number of the upper state population and R_p is the total pump rate. Similarly, the spatial distribution $\phi(\mathrm{r},t)$ can be expressed as $\phi(\mathrm{r},t) = \Phi\phi_o(\mathrm{r})$, where $\phi_o(\mathrm{r})$ is the normalized distribution of the cavity mode and F is the total number of the cavity photons. Multiplying $\phi_o(\mathrm{r})$ on both sides of Equation (2) and integrating the space, we can obtain

$$\frac{d\,N}{dt} = R_p - \frac{c\sigma\,\Phi N}{SV_{eff}} - \frac{N}{\tau_f}, \tag{3}$$

where the slope efficiency S and the effective mode volume V_{eff} are given by [16,17]

$$S = \frac{\left[\iiint \rho_o(\mathrm{r})\,\phi_o(\mathrm{r})d^3r\right]^2}{\iiint \rho_o(\mathrm{r})\,\phi_o{}^2(\mathrm{r})d^3r}, \tag{4}$$

$$V_{eff} = \left[\iiint \rho_o(\mathrm{r})\,\phi_o(\mathrm{r})d^3r\right]^{-1}. \tag{5}$$

The rate equation for the cavity photon number F can be given by

$$\frac{d\Phi}{dt} = c\sigma\,\Phi \iiint n(\mathbf{r},t)\,\phi_o(\mathbf{r})d^3r \; - \frac{\Phi}{\tau_c}, \tag{6}$$

where $\tau_c = t_r/(T+L)$ is the lifetime of the cavity photon, t_r is the round-trip time of the cavity photon, L is the internal round-trip losses, and T is the output transmittance. Substituting $n(\mathrm{r},t) = N\rho_o(\mathrm{r})$ into Equation (6) and in terms of V_{eff}, the rate equation for the photon number F can be expressed as

$$\frac{d\Phi}{dt} = \frac{c\sigma\,\Phi N}{V_{eff}} \; - \frac{\Phi}{\tau_c}\,. \tag{7}$$

The critical population number N_{th} for the steady-state operation can be derived by setting $d\Phi/dt = 0$ in Equation (7) to obtain

$$N_{th} = \frac{V_{eff}}{c\sigma\tau_c}\,. \tag{8}$$

The critical number $N = N_{th}$ can be applied to Equation (3) with $dN/dt = 0$ and $\Phi = 0$ to obtain the threshold pump rate given by $R_{p,th} = N_{th}/\tau_f$, i.e.,

$$R_{p,th} = \frac{V_{eff}}{c\sigma\tau_f\tau_c} = \frac{(T+L)}{c\sigma\,\tau_f\;t_r}\,V_{eff}. \tag{9}$$

The threshold pump power can be obtained as

$$P_{th} = (h\nu_p)R_{p,th} = \frac{(T+L)}{2l_{cav}}\frac{(h\nu_p)}{(h\nu_l)}I_{sat}\,V_{eff}, \tag{10}$$

where $I_{sat} = (h\nu_l)/(\sigma\tau_f)$, $h\nu_p$ is the pump photon energy, and $h\nu_l$ is the lasing photon energy. For the steady-state operation, the population number N is clamped at the pump threshold. Consequently, using Equation (3) with $d\,N/dt = 0$ and $N = N_{th}$, we can express the cavity photon number as

$$\Phi = \frac{SV_{eff}}{c\sigma\,N_{th}}\Big(R_p - R_{p,th}\Big). \tag{11}$$

The pump rate can be expressed as $R_p = P_{IN}/h\nu_p$, where P_{IN} is the incident pump power. Using Equations (8)–(11), the intracavity power P_{CA} can be derived as

$$P_{CA} = \frac{h\nu_l}{t_r}\Phi = \frac{1}{(T+L)}\frac{(h\nu_l)}{(h\nu_p)}S(P_{IN} - P_{th}). \tag{12}$$

In terms of P_{CA}, the intracavity pulse energy can be expressed as $P_{CA}\,t_r$. The critical pump power for achieving CWML is denoted as $P_{IN,C}$, which can be analytically deduced by using Equations (1) and (12) with the condition of $P_{CA}\,t_r = E_{p,C}$. Accordingly, the condition for the critical pump power $P_{IN,C}$ can be given by

$$\frac{t_r}{(T+L)}\frac{(h\nu_l)}{(h\nu_p)}S(P_{IN,C} - P_{th}) = E_{p,c}. \tag{13}$$

The critical pump power $P_{IN,C}$ can be consequently expressed as

$$P_{IN,C} = P_{th} + \frac{(T+L)}{S}\frac{v_p}{v_l}\frac{E_{P,C}}{t_r}. \tag{14}$$

Since P_{th} is generally significantly smaller than $P_{IN,C}$, the critical pump power is mainly dominated by the second term in Equation (14), which is relevant to $E_{P,C}$.

Considering the fiber-coupled diode-end-pumped solid-state lasers, the pump beam can be modeled as cylindrical symmetry. The normalized distributions of the pump beam and cavity mode can be given by

$$\rho_o(\mathrm{r}) = \frac{\alpha e^{-\alpha z}}{1 - e^{-\alpha l_{cry}}} \frac{2}{\pi \omega_p^2(z)} e^{-2(x^2+y^2)/\omega_p^2(z)}, \tag{15}$$

$$\phi_o(\mathrm{r}) = \frac{1}{l_{cav}} \frac{2}{\pi \omega_c^2(z)} e^{-2(x^2+y^2)/\omega_c^2(z)}, \tag{16}$$

where a is the absorption coefficient of the gain medium for the pump light, l_{cry} is the length of the gain medium, $\omega_p(z)$ is the radius of the pump beam, and $\omega_c(z)$ is the radius of the cavity mode. The z-dependence of $\rho_o(\mathrm{r})$ and $\phi_o(\mathrm{r})$ can be approximately replaced with the average values $\overline{\omega}_p$ and $\overline{\omega}_c$ for the pump and mode radii, respectively. The accuracy of using average values $\overline{\omega}_p$ and $\overline{\omega}_c$ for the analysis has been numerically confirmed in previous work [16]. In terms of $\overline{\omega}_p$ and $\overline{\omega}_c$, the threshold pump power P_{th} and the slope efficiency S can be analytically expressed as

$$P_{th} = (T + L) \frac{h\upsilon_p}{\sigma \tau_f} \frac{\pi\left(\overline{\omega}_p^2 + \overline{\omega}_c^2\right)}{4}, \tag{17}$$

$$S = \frac{\left(2\overline{\omega}_p^2 + \overline{\omega}_c^2\right)\overline{\omega}_c^2}{\left(\overline{\omega}_p^2 + \overline{\omega}_c^2\right)^2}. \tag{18}$$

If the pump source is not symmetric in the transverse plane, the normalized distributions of the pump beam can be modeled as

$$\rho_o(\mathrm{r}) = \frac{\alpha e^{-\alpha z}}{1 - e^{-\alpha l_{cry}}} \frac{2}{\pi \sqrt{\omega_{p,x}(z)\omega_{p,y}(z)}} e^{-2x^2/\omega_{p,x}^2(z)} e^{-2y^2/\omega_{p,y}^2(z)}. \tag{19}$$

As a consequence, the threshold pump power P_{th} and the slope efficiency S can be modified as

$$P_{th} = (T + L) \frac{h\upsilon_p}{\sigma \tau_f} \frac{\pi}{4} \sqrt{\overline{\omega}_{p,x}^2 + \overline{\omega}_c^2} \sqrt{\overline{\omega}_{p,y}^2 + \overline{\omega}_c^2}, \tag{20}$$

$$S = \frac{\sqrt{(2\overline{\omega}_{p,x}^2 + \overline{\omega}_c^2)}\sqrt{(2\overline{\omega}_{p,y}^2 + \overline{\omega}_c^2)}\,\overline{\omega}_c^2}{(\overline{\omega}_{p,x}^2 + \overline{\omega}_c^2)(\overline{\omega}_{p,y}^2 + \overline{\omega}_c^2)}, \tag{21}$$

where $\overline{\omega}_{p,x}$ and $\overline{\omega}_{p,y}$ are the average pump radii in the x and y direction, respectively. In the following section, the theoretical analysis for the critical pump power $P_{IN,C}$ will be performed by using Equations (1), (14), (17) and (18).

3. Cavity Design

Currently, the cavity configurations for implementing passive mode-locked solid-state lasers mainly include V-shaped [18], Z-shaped [19], W-shaped [20], and V–Z-shaped [21] structures. Although there are different cavity configurations, the basic concerns for achieving stable CWML are almost the same to consider as the total cavity length, as well as the mode sizes on the laser crystal and the saturable absorber. Nevertheless, it is practically useful to construct the mode-locked cavity as simple as possible. In this work, we develop a practical and prompt way to design passively mode-locked solid-state lasers, as shown in Figure 1 for the cavity configuration. The laser cavity comprises a gain medium, a saturable absorber, and a focusing lens to keep the overall components as minimal as possible. Here,

the gain medium was an *a*-cut Nd:YVO_4 crystal with a dopant concentration of 0.35 at.% and a size of $3 \times 3 \times 8$ mm^3 (CASTECH Inc., Fuzhou, China). The first side of the gain medium was polished as a plane facet and was coated to be a cavity mirror with high transmission (HT) for the pump light at 808 nm (transmittance > 95%) and high reflection (HR) for the laser wavelength at 1064 nm (reflectance > 99.8%). The second facet of the gain medium was polished with a wedged angle of 0.5° to eliminate the internal etalon effect and was coated to be anti-reflective (AR) at 1064 nm (reflectance < 0.2%). The saturation fluence of the gain medium was $F_{sat,L} = 3.66 \times 10^7$ nJ/cm^2. The gain medium was wrapped with indium foil and was closely packaged in a copper block with water cooling at a temperature of 20 °C. A fiber-coupled laser diode with a wavelength of 808 nm was used as the pump source. The core radius and numerical aperture of the coupled fiber were 100 μm and 0.16, respectively. The pump imaging optics consisted of a collimating lens with a focal length of 25 mm and a focusing lens with a focal length of 50 mm to produce an average pump radius of 250 mm in the crystal. The saturable absorber was a SESAMOC that simultaneously acted as an SESAM device, an output coupler [22,23]. Two different SESAMOC chips were prepared for experiments. The SESAM device was homemade and based on an undoped GaAs substrate with the method of metalorganic chemical vapor deposition. The SESAMOC included 10 pairs of distributed Bragg reflectors (DBRs) that were formed by AlAs/GaAs quarter-wavelength layers with an effective reflectivity of approximately 96.5% at 1064 nm. The absorbing material of the SESAMOC was made of an 8-nm $In_{0.34}Ga_{0.66}As$ quantum well. Note that the actual cavity was formed by DBRs. The characteristics of the first SESAMOC chip were $T = 4.5$ %, $F_{sat,A} = 3 \times 10^4$ nJ/cm^2, and $\Delta R = 0.01$. The characteristics of the second SESAMOC chip were $T = 5.0$ %, $F_{sat,A} = 5 \times 10^4$ nJ/cm^2, and, $\Delta R = 0.02$. The back facets of the SESAMOC chips were coated to be AR at 1064 nm (reflectance < 0.5%). In the experiment, the SESAMOC chip was soldered on a copper holder with water cooling at a temperature of 20 °C. An intracavity plano-convex lens with a focal length of $f = 150$ mm was exploited to generate a variety of $A_{eff,L}$ and $A_{eff,A}$. The critical pump powers $P_{IN,C}$ for achieving CWML were systematically measured to compare with the theoretical analysis.

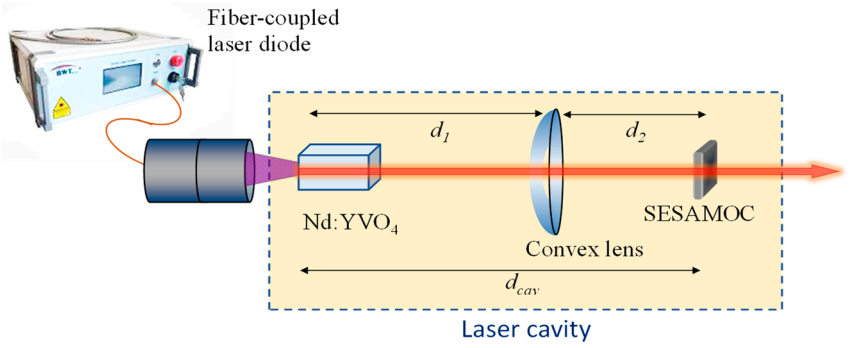

Figure 1. Cavity scheme for designing passively mode-locked solid-state lasers.

The experimental optical spectra were measured using a Michelson interferometer with a Fourier spectrometer (Advantest Q8347, Tokyo, Japan), with a resolution as high as 0.003 nm. A high-speed InGaAs photodetector (Electro-optics Technology Inc. ET-3500, Edinburgh, UK) with rise time 35 ps was used to measure the temporal properties of the mode-locked laser, and a digital oscilloscope (Teledyne LeCroy, Wave Master 820Zi-A, Bucks, UK) was used to record its output signal. In addition, the output signal detected by the photodetector was used to analyze the output power spectrum based on an RF spectrum analyzer (Agilent, 8563EC, Santa Clara, CA, USA), with a bandwidth of 26.5 GHz to measure. A commercial autocorrelator (APE Pulse Check, Angewandte Physik and Elektrnic GmbH, Göppingen, Germany) was used to measure second-order autocorrelation traces for analyzing the effective pulse duration.

The mode areas $A_{eff,L}$ and $A_{eff,A}$ for the proposed cavity can be obtained from the ABCD matrix method. Accordingly, the radius of the cavity mode at the pump side of the gain medium can be derived as

$$w_1 = \sqrt{\frac{\lambda}{\pi}\sqrt{\frac{(d_1 - f)[(d_1 + d_2)f - d_1 d_2]}{(d_2 - f)}}}, \tag{22}$$

where l is the laser wavelength, d_1 is the optical length between the pump side of the gain medium and the focusing lens, and d_2 is the optical length between the focusing lens and the SESAMOC chip. On the other hand, the radius of the cavity mode at the SESAMOC chip can be derived as

$$w_2 = \sqrt{\frac{\lambda}{\pi}\sqrt{\frac{(d_2 - f)[(d_1 + d_2)f - d_1 d_2]}{(d_1 - f)}}}. \tag{23}$$

For convenience, the distance d_1 was fixed at 310 mm and the distance d_2 was varied in the experiment. Figure 2 shows the calculated results for the mode radii w_1 and w_2 as a function of the distance d_2 with d_1 = 310 mm. The mode radii w_1 and w_2 can be seen to simultaneously decrease with an increasing distance d_2 in the range between 230 mm and 290 mm. Accordingly, the dependence of the critical pump power on the mode radii w_1 and w_2 can be experimentally explored in this range. Since the mode radius w_1 in the range out of d_2 =230–290 mm significantly grows upward, the threshold pump power for CWML will be too high to achieve the mode-locked operation.

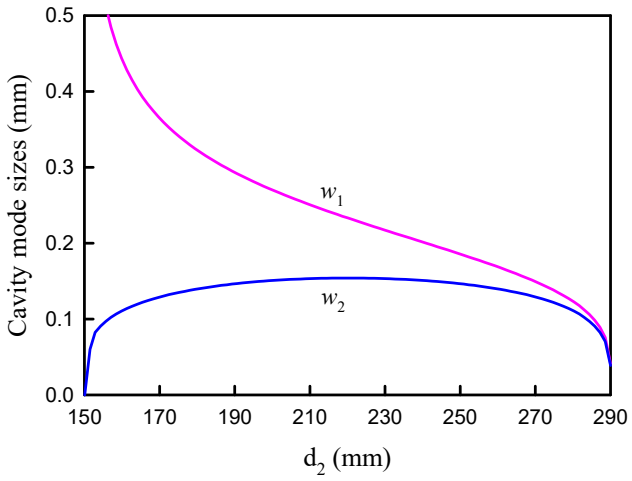

Figure 2. Calculated results for the mode radii w_1 and w_2 as a function of d_2 with d_1 = 310 mm.

4. Results and Discussion

First of all, the mode-locked operation was optimized with the first SESAMOC chip at d_2 = 280 mm. As seen in Figure 3a, the critical pump power $P_{IN,C}$ for CWML is approximately 1.0 W. Figure 3b shows the temporal characteristics of the QML and CWML. Figure 3c–f show the output performance obtained with the pump power of 3.0 W. Note that the overall output characteristics are almost unchanged for $P_{IN,C} < P_{IN} < 7$ W. From Figure 3c for the RF power spectrum in the range of 5 GHz, the overall signal-to-noise ratio for the first several peaks can be seen to be considerably higher than 50 dB. Figure 3d shows the RF power spectrum in the range of 5 MHz to reveal the side-mode suppression ratio (SMSR), which is defined as the difference between the main oscillation mode and the highest side mode. The SMSR can be seen to be higher than 50 dB. The sideband of the RF spectrum mainly comes from the relaxation oscillation, which is the characteristic phenomenon of most solid-state lasers where the recovery time of the population inver-

sion of the excited state is much longer than the cavity decay time. Figure 3e shows the lasing optical spectrum. The full width at half-maximum (FWHM) can be found to be approximately 0.09 nm. The modulation characteristics in the lasing spectrum mainly come from the residual etalon effect between the internal focus lens and the SESAMOC device. Figure 3f shows the intensity autocorrelation traces. Based on the Gaussian fitting, the pulse width is 20.1 ps, leading to a time-bandwidth product of 0.48, which is close to the transform limit of 0.441. Under the optimal alignment, the critical pump power for CWML was measured while varying the distance d_2 from 230 to 280 mm.

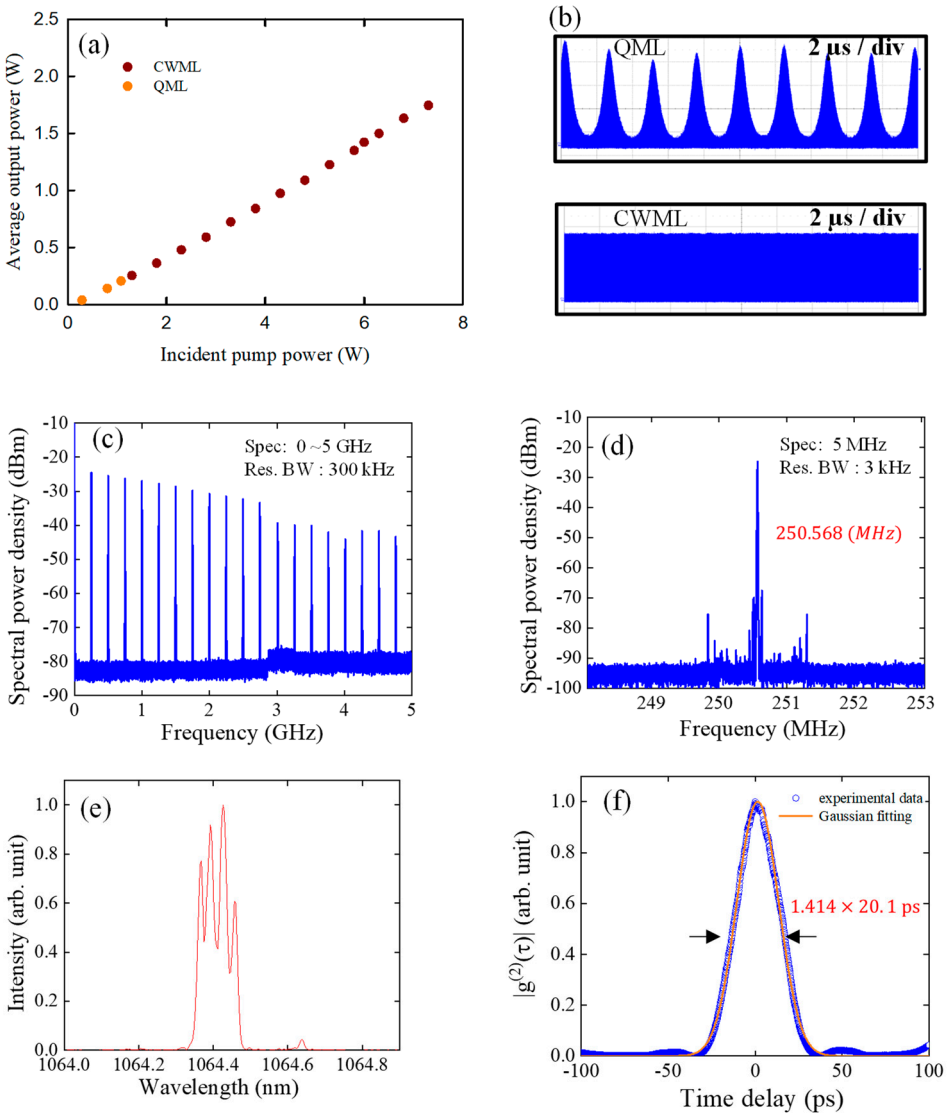

Figure 3. (**a**) Average output power versus pump power indicating QML and CWML operations obtained with the first SESAMOC chip. (**b**) Temporal characteristics of the QML and CWML. (**c**) RF power spectrum in the range of 5 GHz. (**d**) RF power spectrum in the range of 5 MHz. (**e**) Optical lasing spectrum. (**f**) Intensity autocorrelation traces.

The same experiment was also performed with the second SESAMOC chip. The overall output characteristics are shown in Figure 4 with a presentation similar to Figure 3. From Figure 4a, the critical pump power $P_{IN,C}$ for CWML can be seen to be around 2.1 W, which is obviously higher than the result obtained with the first SESAMOC chip. Figure 4b shows the temporal characteristics of the QML and CWML. Figure 4c–f show the experimental results obtained with the pump power of 3.0 W. Once again, the overall output characteristics are nearly unchanged for $P_{IN,C} < P_{IN} < 7$ W. Compared with the results

obtained with the first SESAMOC chip, the main differences consist of the lasing spectral width and pulse duration. From Figure 4e,f, the FWHM values for the lasing spectrum and pulse duration can be seen to be approximately 0.16 nm and 10.8 ps, respectively. Once again, the modulation feature in the lasing spectrum is mainly due to the residual etalon effect between the internal focus lens and the SESAMOC device. Consequently, the time-bandwidth product was around 0.46, which is closer to the transform limit of 0.441. Similarly, the critical pump power for CWML was measured while varying the distance d_2 from 230 to 280 mm.

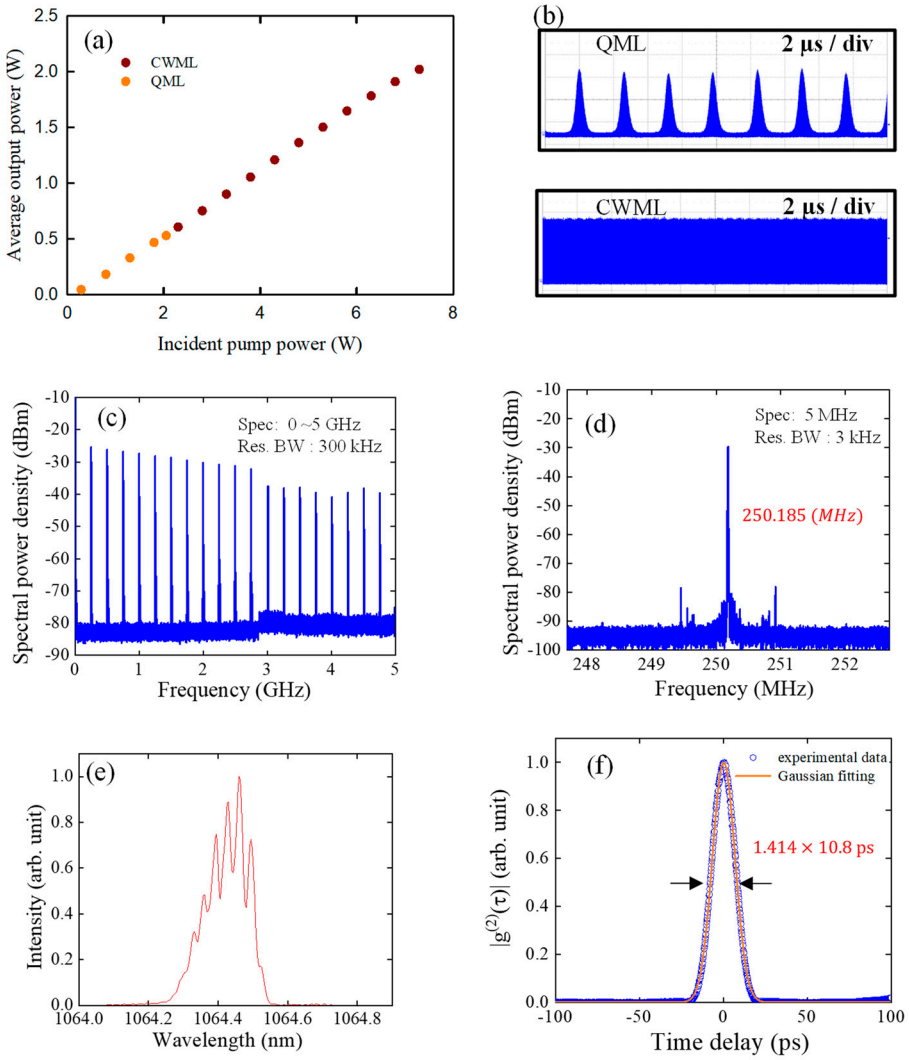

Figure 4. (**a**) Average output power versus pump power indicating QML and CWML operations obtained with the second SESAMOC chip. (**b**) Temporal characteristics of the QML and CWML. (**c**) RF power spectrum in the range of 5 GHz. (**d**) RF power spectrum in the range of 5 MHz. (**e**) Optical lasing spectrum. (**f**) Intensity autocorrelation traces.

The resulting mode-locked laser operates stably over 24 h with low timing jitter and low noise. It was also confirmed that the self-starting operation is reproducible from day to day. Figure 5 shows the comparison between the experimental and theoretical results for the critical pump powers varying with the distance d_2. The theoretical calculations were performed with $A_{eff,L} = \pi w_1^2/2$, $A_{eff,A} = \pi w_2^2/2$, $\overline{\omega}_c = w_1$, $\overline{\omega}_p = 0.25$ mm, and $L = 0.01$. Here, the value of $\overline{\omega}_p$ was determined from the focusing of the pump beam, and the value of L was estimated from the lasing threshold. The theoretical calculations can be found to agree very well with the experimental data. The good agreement between the numerical calculations and the experimental measurements confirms the validity of the

theoretical analyses. It is worthwhile to mention that even though a larger modulation depth leads to a higher critical pump power, it can bring about a shorter pulse width in return. The thermal stability of the cavity setup is an important issue for practical design. In the following section, a comprehensive analysis for the thermal stability of the proposed cavity is provided to help readers obtain excellent performance.

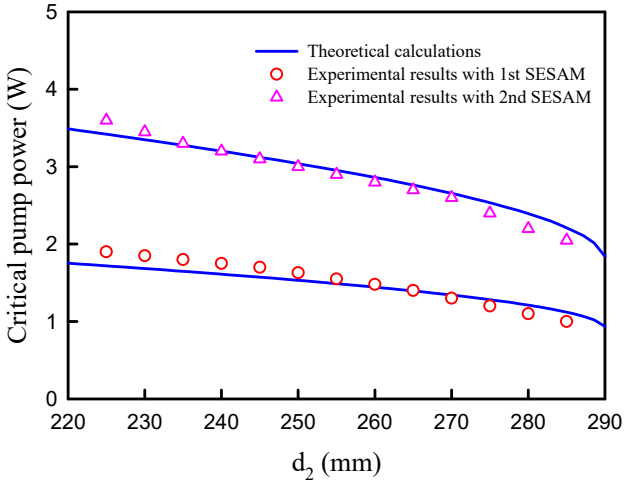

Figure 5. Comparison between the experimental and theoretical results for the critical pump powers varying with the distance d_2.

5. Analysis of Thermal Stability

To analyze the thermal stability of the proposed cavity, the laser crystal can be characterized as a lens-like medium. The effective focal length of the laser crystal is assumed to be given by f_{th}. As a consequence, the round trip for a resonator formed by the flat mirrors with an internal lens and a thermal lens-like medium can be written as

$$\begin{bmatrix} A & B \\ C & D \end{bmatrix} = \begin{bmatrix} 1 & 0 \\ -\frac{1}{f_{th}} & 1 \end{bmatrix} \begin{bmatrix} 1 & d_1 \\ 0 & 1 \end{bmatrix} \begin{bmatrix} 1 & 0 \\ -\frac{1}{f} & 1 \end{bmatrix} \begin{bmatrix} 1 & 2d_2 \\ 0 & 1 \end{bmatrix} \begin{bmatrix} 1 & 0 \\ -\frac{1}{f} & 1 \end{bmatrix} \begin{bmatrix} 1 & d_1 \\ 0 & 1 \end{bmatrix} \begin{bmatrix} 1 & 0 \\ -\frac{1}{f_{th}} & 1 \end{bmatrix}. \quad (24)$$

After some algebra, the matrix elements A and D can be derived as

$$A = D = 1 - \frac{2}{f}\left(d_1 + d_2 - \frac{d_1 d_2}{f}\right)\left(1 + \frac{f - d_1}{f_{th}}\right). \quad (25)$$

The criterion for a stable resonator is given by

$$-1 \leq \frac{A + D}{2} \leq 1. \quad (26)$$

Substituting Equation (25) into Equation (26), the criterion for a stable cavity can be expressed as

$$0 \leq \frac{1}{f}\left(d_1 + d_2 - \frac{d_1 d_2}{f}\right)\left(1 + \frac{f - d_1}{f_{th}}\right) \leq 1. \quad (27)$$

For clear discussion, we assume to be given a fixed length d_1 and a focal length f. The length d_1 is conveniently in terms of the focal length f as $d_1 = M \cdot f$. Namely, the parameter M is the ratio of d_1 to f. The condition for a stable resonator under the thermal lensing effect can be further analyzed by substituting $d_1 = M \cdot f$ into Equation (27). As a result, the criterion for the thermal stability can be given by

$$0 \leq \left[M - (M-1)\frac{d_2}{f}\right]\left[1 - (M-1)\frac{f}{f_{th}}\right] \leq 1. \quad (28)$$

Without the thermal lensing effect, $f_{th} \to \infty$, Equation (28) can be deduced as the criterion of the length d_2, which is given by

$$f \ \leq \ d_2 \ \leq \ \left(\frac{M}{M-1}\right) f. \tag{29}$$

When the thermal lensing effect is less than the strength of $(M-1)f < f_{th}$, the stable range for the length d_2 can be derived as

$$f\left[1 - \frac{f}{f_{th} - (M-1)f}\right] \ \leq d_2 \ \leq \ \left(\frac{M}{M-1}\right) f. \tag{30}$$

This result reveals that the length d_2 needs to be shorter than the critical value of $d_c = M \cdot f/(M-1)$. In particular, if the strength of the thermal lensing effect is within $(M-1)f < f_{th} < M \cdot f$, the stable range for the length d_2 can be simplified as

$$0 \ \leq d_2 \ \leq \ \left(\frac{M}{M-1}\right) f. \tag{31}$$

In comparison with Equation (29), the result of Equation (31) indicates that the lower bound for the length d_2 can be extended from f down to zero with the help of the thermal lensing effect. It is clear that the stable region given by Equation (31) is always wider than the region without the thermal effect given by Equation (29). As a consequence, the cavity can be maintained to be stable as long as the effective focal length f of the thermal lensing is greater than $(M-1)f$. To be brief, when the effective focal length f_{th} is longer than the critical strength $(M-1)f$, the cavity can be maintained to be stable. On the other hand, when the thermal lensing effect is greater than the strength of $(M-1)f > f_{th}$, the range of the length d_2 for a stable cavity is changed as

$$\left(\frac{M}{M-1}\right) f \leq \ d_2 \ \leq \ f\left[1 - \frac{f}{f_{th} - (M-1)f}\right]. \tag{32}$$

It is clear that the stable range of the length d_2 switches to the region longer than the critical value of $d_c = M \cdot f/(M-1)$.

6. Conclusions

In summary, we started from the spatially dependent rate equations to derive an analytical equation for the output power as a function of the pump power. We linked the derived equation with the critical intracavity pulse energy to obtain an analytical expression for evaluating the critical pump power for achieving CWML. Furthermore, a prompt way was proposed to straightforwardly design the cavity for passively mode-locked solid-state lasers. We not only experimentally demonstrated the proposed cavity design but also numerically verified the theoretical analysis for the critical pump powers. We also intriguingly found that although a larger modulation depth leads to a higher critical pump power, it can generate a shorter pulse width in return. Finally, we made a comprehensive analysis of the thermal stability of the proposed cavity to obtain excellent performance.

Author Contributions: Conceptualization, P.-W.C. and Y.-F.C.; validation, P.-W.C. and H.-C.L.; formal analysis, P.-W.C. and Y.-F.C.; resources, Y.-H.H. and K.-F.H.; writing—original draft preparation, Y.-F.C.; writing—review and editing, P.-W.C., H.-C.L. and Y.-F.C.; supervision, Y.-F.C. All authors have read and agreed to the published version of this manuscript.

Funding: This work is supported by the National Science and Technology Council of Taiwan (contract number 112-2112-M-A49-022-MY3).

Institutional Review Board Statement: Not applicable.

Informed Consent Statement: Not applicable.

Data Availability Statement: All data reported in this paper are presented in the main text. Any other data will be provided upon request.

Conflicts of Interest: The authors declare no conflicts of interest.

References

1. Kleinbauer, J.; Knappe, R.; Wallenstein, R. A powerful diode-pumped laser source for micro-machining with ps pulses in the infrared, the visible and the ultraviolet. *Appl. Phys. B* **2005**, *80*, 315. [CrossRef]
2. Major, A.; Sandkuijl, D.; Barzda, V. Efficient frequency doubling of a femtosecond Yb:KGW laser in a BiB_3O_6 crystal. *Opt. Express* **2009**, *17*, 12039–12042. [CrossRef] [PubMed]
3. Zhao, H.; Lima, I.T., Jr.; Major, A. Near-infrared properties of periodically poled $KTiOPO_4$ and stoichiometric MgO-doped $LiTaO_3$ crystals for high power optical parametric oscillation with femtosecond pulses. *Laser Phys.* **2010**, *20*, 1404–1409. [CrossRef]
4. Qiao, W.; Chu, H.; Wang, Z.; Zhao, S.; Li, G.; Yang, K.; Li, T.; Zhao, J.; Zhang, B.; He, J. Mode-locking characteristics comparison at 1.34 μm between Nd:$Gd_xY_{1-x}VO_4$ series crystals. *Laser Phys.* **2016**, *26*, 045801. [CrossRef]
5. Kasparian, J.; Wolf, J.P. Ultrafast laser spectroscopy and control of atmospheric aerosols. *Phys. Chem. Chem. Phys.* **2012**, *14*, 9291. [CrossRef]
6. Kaminskii, A.A.; Zhang, J.; Lux, O.; Rhee, H.; Eichler, H.J.; Tang, D.V.; Yu, H.H.; Zhang, H.J.; Wang, J.; Yoneda, H.; et al. Stimulated Raman scattering spectroscopy of $Y_{0.4}Gd_{0.6}VO_4$ crystals with partly disordered zircon-type structure—Observation of new $\chi^{(3)}$-nonlinear optical interactions. *Laser Phys. Lett.* **2014**, *11*, 125808. [CrossRef]
7. Cai, Z.; Wen, W.; Wang, Y.; Zhang, Z.; Ma, X.; Ding, X.; Yao, J. 5.3-W Nd:YVO_4 passively mode-locked laser by a novel semiconductor saturable absorber mirror. *Chin. Opt. Lett.* **2005**, *3*, 342–344.
8. Fan, Y.-X.; He, J.-L.; Wang, Y.-G.; Liu, S.; Wang, H.-T.; Ma, X.-Y. 2-ps passively mode-locked Nd: YVO_4 laser using an output-coupling-type semiconductor saturable absorber mirror. *Appl. Phys. Lett.* **2005**, *86*, 101103. [CrossRef]
9. Xie, G.; Tang, D.; Tan, W.; Luo, H.; Zhang, H.; Yu, H.; Wang, J. Subpicosecond pulse generation from a Nd: CLNGG disordered crystal laser. *Opt. Lett.* **2009**, *34*, 103–105. [CrossRef]
10. Sun, L.; Yu, H.J.; Zhang, L.; Guo, L.; Zhang, J.; Dong, Z.Y.; Xiong, B.; Hou, W.; Lin, X.C.; Li, J.M. High efficiency passive mode-locked Nd:YVO_4 laser based on SESAM under direct pumping at 880 nm. *Laser Phys.* **2011**, *21*, 1765–1768. [CrossRef]
11. Hönninger, C.; Paschotta, R.; Morier-Genoud, F.; Moser, M.; Keller, U. *Q*-switching stability limits of continuous-wave passive mode locking. *J. Opt. Soc. Am. B* **1999**, *16*, 46–56. [CrossRef]
12. He, J.; Liu, J.; Du, J.; Yang, J.; Man, B. Low-threshold and highly efficient diode-pumped cw passively mode-locked Nd:YVO_4 laser with a saturable Bragg reflector. *Opt. Eng.* **2005**, *44*, 094201. [CrossRef]
13. Rao, H.; Cong, Z.H.; Qin, Z.G.; Feng, C.; Wang, Q.P.; Liu, Z.J.; Zhang, X.Y.; Zhang, S.S.; Liu, Y.; Men, S.J.; et al. A diode pumped passively mode-locked Nd:$CaGdAlO_4$ laser. *Laser Phys.* **2016**, *26*, 045802. [CrossRef]
14. Shi, Y.; Li, J.; Yang, J.; Ouellette, F.; Zhu, C.; Peng, H.; Liu, Y. Passively Q-Switched 3-μm Ho^{3+}-Doped Fiber Laser Based on Nonlinear Polarization Rotation. *IEEE Photonics Technol. Lett.* **2019**, *31*, 1437–1440. [CrossRef]
15. Zheng, J.-C.; Yang, S.; Zhu, Z.-W.; Lau, K.-Y.; Li, L. 72-fs Er-doped Mamyshev Oscillator. *J. Light. Technol.* **2021**, *40*, 2123–2127. [CrossRef]
16. Chen, Y.F.; Liao, T.S.; Kao, C.F.; Huang, T.M.; Lin, K.H.; Wang, S.C. Optimization of fiber-coupled laser-diode end-pumped lasers: Influence of pump-beam quality. *IEEE J. Quantum Electron.* **1996**, *32*, 2010–2016. [CrossRef]
17. Chen, Y.F.; Huang, T.M.; Kao, C.F.; Wang, C.L.; Wang, S.C. Optimization in scaling fiber-coupled laser-diode end-pumped lasers to higher power: Influence of thermal effect. *IEEE J. Quantum Electron.* **1997**, *33*, 1424–1429. [CrossRef]
18. Iliev, H.; Buchvarov, I.; Choi, S.Y.; Kim, K.; Rotermund, F.; Petrov, V. 1.34 μm Nd:YVO_4 laser mode-locked by a single-walled carbon nanotube saturable absorber. In Proceedings of the SPIE—Solid State Lasers XXI: Technology and Devices, San Francisco, CA, USA, 22–25 January 2012; Volume 8235, p. 82350I.
19. Liu, Y.H.; Xie, Z.D.; Pan, S.D.; Lv, X.J.; Yuan, Y.; Hu, X.P.; Lu, J.; Zhao, L.N.; Chen, C.D.; Zhao, G.; et al. Diode-pumped passively mode-locked Nd:YVO_4 laser at 1342 nm with periodically poled $LiNbO_3$. *Opt. Lett.* **2011**, *36*, 698–700. [CrossRef]
20. Yang, Y.; Xu, J.-L.; He, J.-L.; Yang, X.-Q.; Zhang, B.-Y.; Yang, H.; Liu, S.-D.; Zhang, B.-T. Diode-pumped passively mode-locked Nd:YAG laser at 1338 nm with a semiconductor saturable absorber mirror. *Appl. Opt.* **2001**, *50*, 6713–6716. [CrossRef]
21. Eibna Halim, M.Z.; Talukder, R.C.; Waritanant, T.; Major, A. Passive mode locking of a Nd:KGW laser with hot-band diode pumping. *Laser Phys. Lett.* **2016**, *13*, 105003. [CrossRef]
22. Huang, T.L.; Li, S.C.; Tsou, C.H.; Liang, H.C.; Huang, K.F.; Chen, Y.F. Narrowing spectral linewidth in passively mode-locked solid-state lasers. *Opt. Lett.* **2018**, *43*, 5753–5756. [CrossRef] [PubMed]
23. Hsu, Y.H.; Cheng, P.W.; Lin, S.Q.; Liang, H.C.; Huang, K.F.; Chen, Y.F. High-peak-power optically pumped passively mode-locked semiconductor laser with minimal components. *Opt. Lett.* **2023**, *48*, 4324. [CrossRef] [PubMed]

Disclaimer/Publisher's Note: The statements, opinions and data contained in all publications are solely those of the individual author(s) and contributor(s) and not of MDPI and/or the editor(s). MDPI and/or the editor(s) disclaim responsibility for any injury to people or property resulting from any ideas, methods, instructions or products referred to in the content.